ADVANCED OPTICAL MATERIALS

Supporting Information

for *Adv. Optical Mater.*, DOI: 10.1002/adom.201600458

Toward Direct Laser Writing of Actively Tuneable 3D Photonic Crystals

*Yaoyang Hu, Benjamin T. Miles, Ying-Lung D. Ho, Mike P. C. Taverne, Lifeng Chen, Henkjan Gersen, John G. Rarity, and Charl F. J. Faul**

Submitted to ADVANCED OPTICAL MATERIALS

Supporting Information

for *Adv. Opt. Mater.*, DOI: 10.1002/adom.201600458

Towards Direct Laser Writing of Actively Tuneable Three-Dimensional Photonic Crystals

*Yaoyang Hu, Benjamin T. Miles, Ying-Lung D. Ho, Mike P. C. Taverne, Lifeng Chen, Henkjan Gersen, John G. Rarity, Charl FJ Faul**

S1. Synthesis of Boc-TANIDA

N-(4-nitrophenyl)-N(4-((4-nitrophenyl)amino)benzene-1,4-diamine (**2**).[30,31]

4,4'-diaminophenylamine (10 g, 33.7 mmol), *p*-nitrofluorobenzene (35.7 mL, 337 mmol) and triethylamine (21 mL) were dissolved in dimethyl sulfoxide (DMSO, 45 mL) in a 250 mL round-bottom flask purged with N_2. After reacting for 24 hours at 90 ^oC, the mixture was poured into deionised water (1 L) resulting in a sticky oil-like material. A red-brown solid was obtained from low pressure filtration, which was subsequently washed with chloroform (100 mL×3), and the sample was dried under vacuum overnight (10.3 g, yield 69%). ^1H NMR (400 MHz, DMSO-d_6, δ): 9.10 (s, 2H, N*H*ArNO), 8.20 (s, 1H, ArN*H*Ar), 8.07-7.98 (m, 4H, Ar*H*), 7.16-7.04 (m, 8H, Ar*H*), 6.94-6.85 (m, 4H, Ar*H*). Elemental analysis calculated for $C_{24}H_{19}N_5O_4$: C 65.30, H 4.34, N 15.86; found: C 64.70, H 4.99, N 14.06.

Tert-butyl(4-((tert-butoxycarbonyl)(4-((tert-butoxycarbonyl)(4-nitrophenyl)amino)phenyl)amino)phenyl)(4-nitrophenyl)carbamate (**3**).[32]

Compound **2** (10.3 g, 23.3 mmol), Boc_2O (23.6 g, 108 mmol) and 4-dimethylaminopyridine (DMAP, 200 mg, 1.63 mmol) was added to a 250 mL N_2-purged round-bottom flask. Tetrahydrofuran (THF, 100 mL) was added to the flask. The reaction was heated to 65 ^oC to allow the solvent to reflux. THF was removed under reduced pressure after 24 hours of reaction. The residue was dissolved in dichloromethane (DCM, 50 mL) and washed by 1 M HCl solution (50 mL) and deionised water (50 mL×3). After drying with anhydrous $MgSO_4$, DCM was removed under reduced pressure and dark red compound **3** was obtained, which was dried under vacuum overnight (14.3 g, yield 83%). ^1H NMR (400 MHz, DMSO-d_6, δ): 8.24-8.12 (m, 4H, Ar*H*), 7.46-7.35 (m, 4H, Ar*H*), 7.31-7.20 (m, 8H, Ar*H*), 1.37 (3s, 27H, CC*H*$_3$). Elemental analysis calculated for $C_{39}H_{43}N_5O_{10}$: C 63.15, H 5.84, N 9.44; found: C 62.97, H 5.86, N 9.32.

Tert-butyl(4-aminophenyl)(4-((4-((4-aminophenyl)(tert-butoxycarbonyl)amino)phenyl)(tert-butoxycarbonyl)amino)phenyl)carbamate (**4**).[32]

Compound **3** (14.3 g, 19.3 mmol), ammonium formate (12.2 g, 193 mmol) and palladium on carbon (5.6 g) were added to a N_2-purged 500 mL round-bottom flask. Dry methanol (100 mL) and dry THF (40 mL) were added to the flask and the reaction mixture was refluxed at 65 ^oC for 5 hours. Complete hydrogenation was confirmed by TLC (eluent: petroleum ether:ethyl acetate = 4:1). THF and methanol were then removed under reduced pressure and the residue dissolved in DCM (50 mL) and filtered through celite. A light pink solid was obtained after DCM was removed. Compound **4** was washed with hexane (100 mL) and dried under vacuum overnight (14.33 g, yield 78%). ^1H NMR (400 MHz, DMSO-d_6, δ): 7.14-7.03 (m, 8H, Ar*H*), 6.86-6.77 (m, 4H, Ar*H*), 6.52-6.44 (m, 4H, Ar*H*), 5.08 (s, 4H, NH_2), 1.33 (3s, 27H, CCH_3). Elemental analysis calculated for $C_{39}H_{47}N_5O_6$: C 68.70, H 6.59, N 10.27; found: C 68.52, H 7.05, N 10.20.

Tert-butyl(4-acrylamidophenyl)(4-((4-((4-acrylamidophenyl)(tert-butoxycarbonyl)-amino)phenyl)(tert-butoxycarbonyl)amino)phenyl)carbamate (Boc-TANI**DA**).

Compound **4** (1 g, 14.7 mmol) was dissolved in dry THF (50 mL) in a 100 mL round-bottom flask that was purged with N_2. Acryloyl chloride (0.238 mL, 4.40 mmol) and triethylamine (TEA, 1 mL) were added to the flask. After reacting for 2 hours at room temperature, the precipitate was filtered off and washed with THF and combined with the organic phase, and the solvent removed under reduced pressure. The residue was dissolved in DCM (30 mL) and washed with 1 M HCl (30 mL), 1 M Na_2CO_3 (30 mL) and deionised water (3×30 mL). After drying with anhydrous $MgSO_4$, DCM was removed under reduced pressure. A yellow solid was obtained after drying under vacuum overnight (yield: 0.95 g, 86.3%). The purity was

confirmed by nuclear magnetic resonance spectroscopy (NMR) and Matrix assist laser desorption ionisation mass spectroscopy (MALDI-MS). Boc-**TANIDA** was analysed by ^{1}H NMR (400 MHz, DMSO-d_6, δ): 10.17 (s, 2H, N*H*CO), 7.69-7.63 (m, 4H, Ar*H*), 7.18-7.10 (m, 12H, Ar*H*), 6.40 (dd, *J* =17.0, 10.1 Hz, 2H, C*H*CH_2), 6.23 (dd, *J* = 17.0, 2.1 Hz, 2H, *trans*-CHCH_2), 5.64 (dd, *J* = 10.1, 2.1 Hz, 2H, *cis*-CHCH_2), 1.35 (3s, 27H, CCH_3); ^{13}C NMR (101 MHz, DMSO-d_6, δ) 163.52, 153.40, 140.82, 140.25, 137.33, 132.19, 128.08, 127.60, 127.38, 120.11, 80.86, 28.24, 28.21. Elemental analysis calculated for $C_{45}H_{51}N_5O_8$: C 68.42, H 6.51, N 8.87; found: C 67.92, H 6.47, N 8.74.

S2. Analysis of Boc-TANIDA

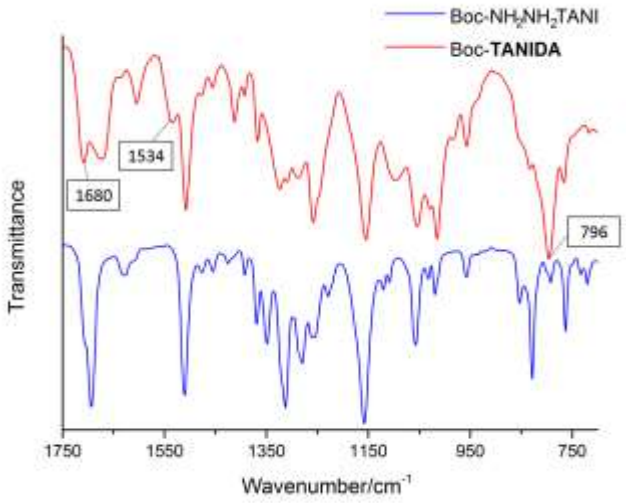

Figure S1 FTIR spectra of Boc-NH_2NH_2**TANI** and Boc-**TANIDA**

FTIR (Fourier transform infrared) further confirmed the polymerisable acrylamide group was attached to the Boc-NH_2NH_2**TANI** moiety. Compared with the spectra in **Figure S1**, three new peaks appeared at 1680 cm^{-1}, 1534 cm^{-1} and 796 cm^{-1}, which represent to C=O and C=C stretching vibrations, and the stretching vibration of the C-H in =C-H, respectively. From the IR spectra it is clear that Boc-**TANIDA** possesses an acrylamide group. In this case, the two acrylamide groups provide crosslinking functionality to **TANI**, which reduced the solubility in isopropanol after polymerisation of Boc-**TANIDA**.

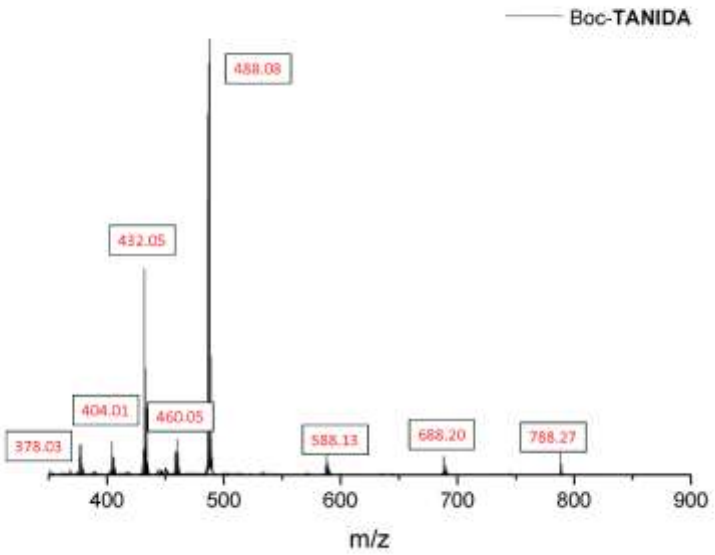

Figure S2 MALDI spectrum of Boc-**TANIDA**

MALDI-MS was applied to confirm the purity of Boc-**TANIDA** (**Figure S2**). Negative ionisation mode was applied when graphite was the matrix. In MALDI spectrum, ion peaks m/z = 788.27, 688.20, 588.13 and 488.08 are respectively [3Boc-**TANIDA** –H]$^-$, [2Boc-**TANIDA** – H]$^-$, [1Boc-**TANIDA** – H]$^-$ and [LEB **TANIDA** – H]$^-$, respectively. There were also four fragments of Boc-**TANIDA**: [LEB acrylate-**TANI**-NCO – H]$^-$ (m/z = 460.04), [EB NH_2-**TANI**-acrylate – H]$^-$ (m/z = 432.05), [EB NH_2-**TANI**-NCO – H]$^-$ (m/z = 404.01) and [EB NH_2-**TANI**-NH_2 – H]$^-$ (m/z = 378.03). Therefore, the spectrum showed that highly pure Boc-**TANIDA** was synthesized.

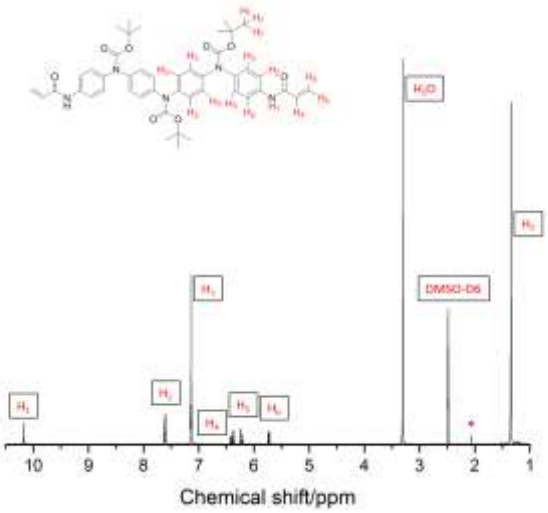

Figure S3 ^{1}H NMR spectrum of Boc-**TANIDA**

The ^{1}H NMR spectrum of Boc-**TANIDA** is shown in **Figure S3**. Distinct resonance peaks at 6.43-5.72 ppm are attributed to the alkene group in the acrylate. A resonance peak at 10.17 ppm appeared, which belongs to the amide proton. The protons in Boc group resonate at 1.34 ppm, whereas the aromatic protons in **TANI** resonate at 7.60-7.13 ppm. The impurity at 2.07 ppm is from acetone. Overall, the NMR spectrum shows the material was synthesized with high purity.

S3. Optimisation of Photoresist Formulation and 2PP Printed Structures

The DLW system used in fabrication is a commercial instrument (Photonic Professional, Nanoscribe GmbH) based on the 2PP technique. It contains a 780 nm femtosecond laser beam (with pulse width of 120 fs and a repetition rate of 80 MHz) focused into Boc-**TANIDA** photoresist by a high numerical aperture (NA = 1.4) oil immersion objective lens (100X, Zeiss).

Table S1 Photoresist formulation optimisation

Formulation	Boc-TANIDA (wt%)	TMPTA (wt%)	BTBPP (wt%)	Concentration in DCM (mg/mL)	Laser power (mW)	Scan speed (µm/s)
F1	86	10	4	10	10	20
F2	86	10	4	30	10	20
F3	86	10	4	50	10	20
F4	56	40	4	50	6	100

The photoresist was optimised from formulation F1 through to formulation F4. It was possible to fabricate structures by formulation F1, but the height of the structures was limited to 1-2 µm. To increase the height of the printed structures, the concentration of the photoresist was increased to 30 mg/mL (formulation F2) and 50 mg/mL (formulation F3), to produce structures with heights of 5.7 µm and 11.0 µm, respectively (**Figure S5**). However, the structures printed with formulation F3 were not stable enough (**Figure S6**), and collapsed. Therefore, the photoresist formulation was further optimised to formulation F4 which was used to fabricate stable structures, as shown in Figure S7 and the main manuscript.

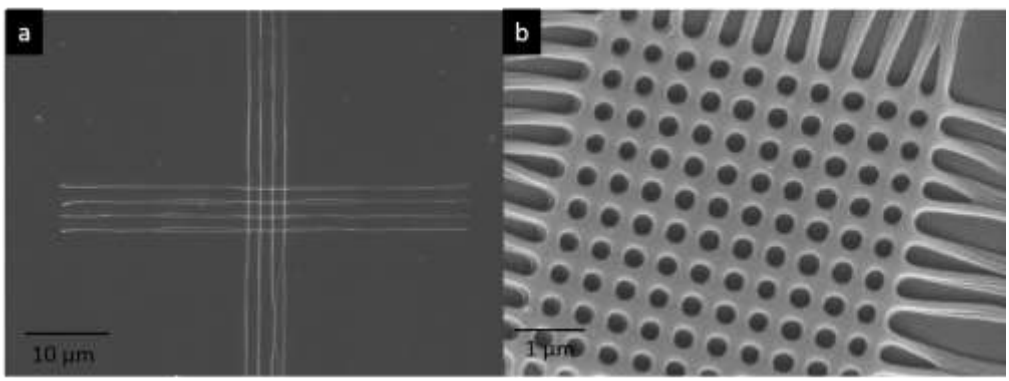

Figure S4 SEM images of 2PP cross structures with photoresist formulation F1: a) cross structure b) cross structure junction.

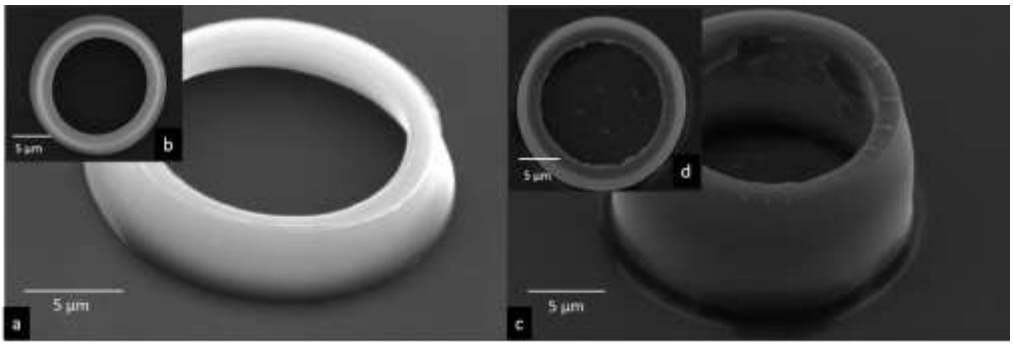

Figure S5 SEM images of 2PP cylinder structures a) printed with photoresist formulation F2, b) printed with photoresist formulation F3.

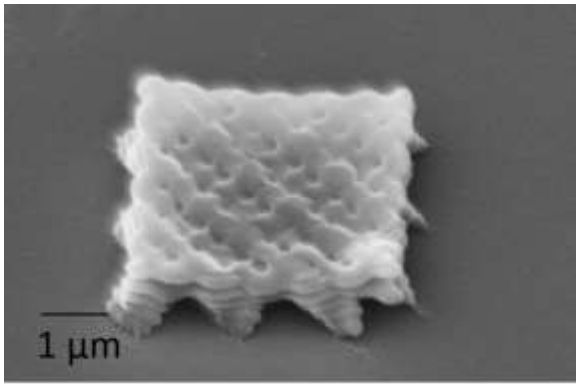

Figure S6 2PP printed structures with photoresist formulation F3: collapsed Tapsterite structure with 5 × 5 array of 3 µm unit-cells.[S1]

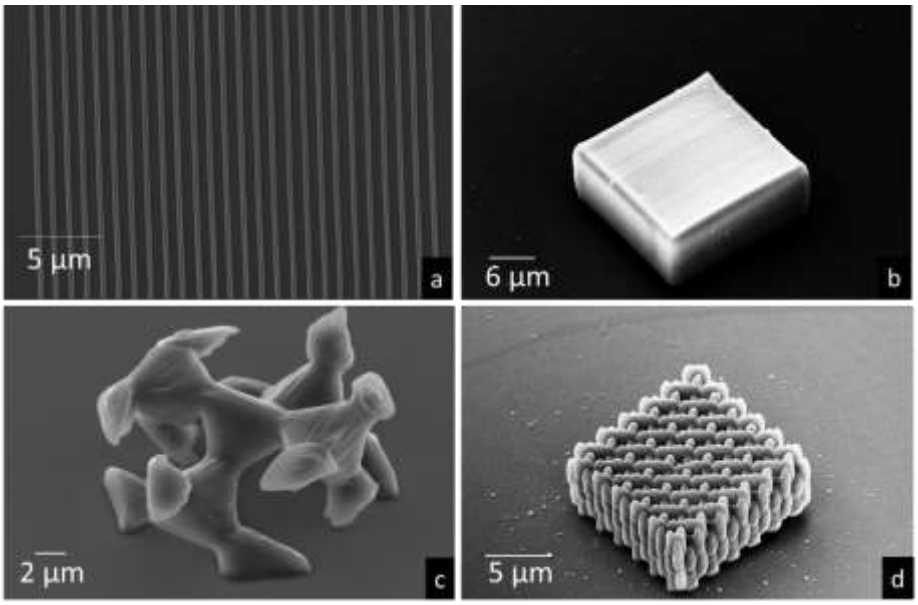

Figure S7 2PP printed structures with photoresist formulation F4 : a) grating structure, b) 2D block structures, c) tapsterite structure with 10 µm unit-cell, d) tapsterite structure with 5 × 5 array of 3 µm unit-cells.[S1]

S4. Design and fabrication parameters of the FCC woodpile structure

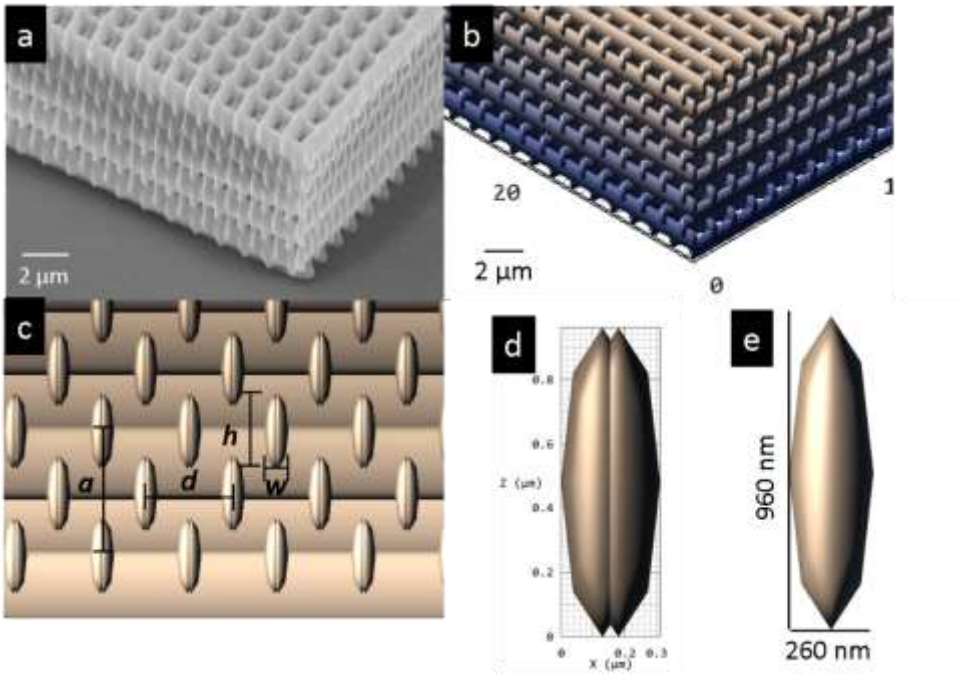

Figure S8 a) SEM image of the 2PP printed FCC woodpile structure. b) and c) images of the modelled woodpile structure, where *a* is the size of the unit-cell, *h* is the rod height, *w* is the rod width and *d* is the distance between rods on the same layer, d) The dimension of a single rod in the modelled woodpile structure with rod width 310 nm and rod height 960 nm. e) The voxel size of the woodpile structure with width 260 nm and height 960 nm.

The woodpile structure was designed to have a FCC (face-centred cubic) geometry. The unit-cell parameter was a_d = 2.235 µm while the distance between rods on the same layers was d_d = $a_d/\sqrt{2}$ ≈ 1.580 µm. Each rod was created from 2 lines separated horizontally by 0.050 µm. There were 5 vertical periods in the woodpile structure, consisting of 4 horizontal layers each (20 in total), and each layer consisted of 18-19 lines. The size of the woodpile structure was designed to be 50 µm long, 50 µm wide and 10 µm high.

Table S2 The parameters of the woodpile structures of design and fabrication.

Parameters (μm)	a	d	w	h
Design of woodpile structures	2.235	1.580	0.500	0.900
Fabricated woodpile structures	1.800	1.273	0.310	0.960

The actual dimensions of the printed woodpile structures are shown in Table S2.The size of unit-cell was a_a = 1.800 μm, the distance between the rods on the same layers was d_a = 1.273 μm, the rod width w_a = 0.310 μm and the rod height was h_a = 0.960 um. The shrinkage factor (a_a/a_d) was = 1.800/2.235 = 0.805.

S5. Voxel size determination

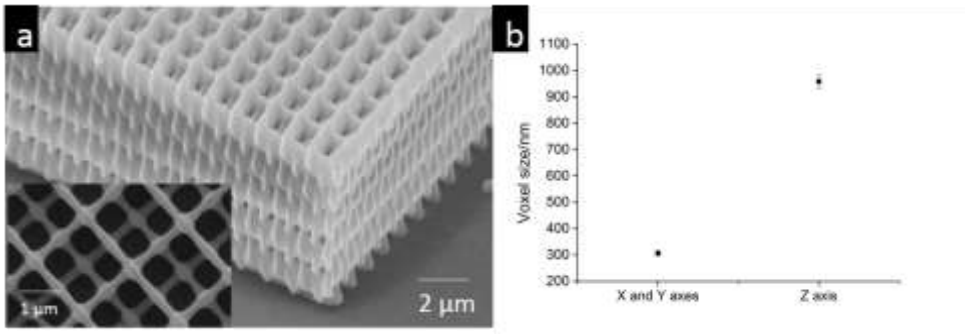

Figure S9 a) The woodpile structure for the rods size measurement, b) rod size of the 2PP printed woodpile structure.

The rod size was estimated from the SEM images of the 2PP printed FCC woodpile structures. ImageJ was used to give a rod width of the woodpile structure of 310 nm and a rod height of 960 nm. Based on the design, the rods of the woodpile structure consisted of 2 lines with a 75% overlap (**Figure S8c**). Hence, the voxel width of the single line is estimated to be 260 nm and the voxel height is 960 nm.

S6. Experimental detail: doping and dedoping process of 2PP printed structures

The 2PP-printed structures were placed at the mouth of open 7 mL vials containing 35 wt% HCl or 35 wt% NH_3 aqueous solutions, respectively, and thus doped and dedoped by vapours from these concentrated solutions.

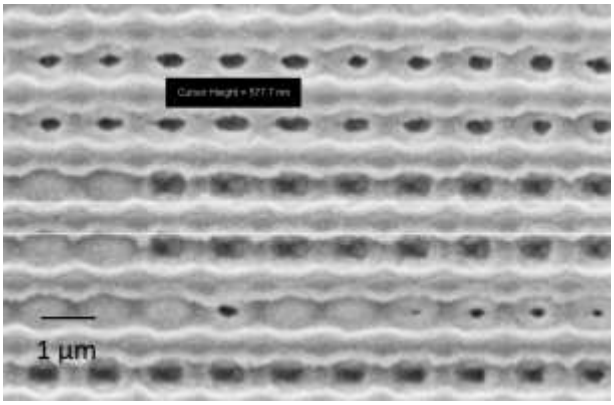

Figure S10 SEM image of the woodpile structures after 5 doping-dedoping cycles.

Ammonium chloride (from the successive acid-base doping/de-doping cycles) coated the woodpile structures after the 5 doping-dedoping cycles (Figure S10), with consequent loss of definition of the printed structure. The ammonium chloride coating was caused by the accumulation of HCl gas and ammonia gas during the doping-dedoping process.

S7. Detail of the calculated slopes

Measurement of phase-delay as a function of position have been performed with a custom-built imaging type Mach-Zehnder interferometer that scans a wedge in XYZ with nanometre precision with a spatial resolution of ~ 220 nm at the wavelength used (532 nm).

The stated height variation of < 100nm is not based on the resolution of the DLW, but is instead based on a combination of other techniques. Firstly, imaging these structures with SEM both before and after doping and de-doping is used to confirm that the overall dimensions remain the same, as stated in the text. This also enables us to determine the height variation (equal to surface roughness). At the same time the Imaging MachZehnder interferometer images the phase-delay as a function of position with ~ 220nm resolution. The variations observed in the phase-delay as a function of position are consistent with the stated < 100 nm variations using the refractive index retrieved from the wedge as a whole. Further experimental details on the microscope used can be found in B.T. Miles *et al*.[35]

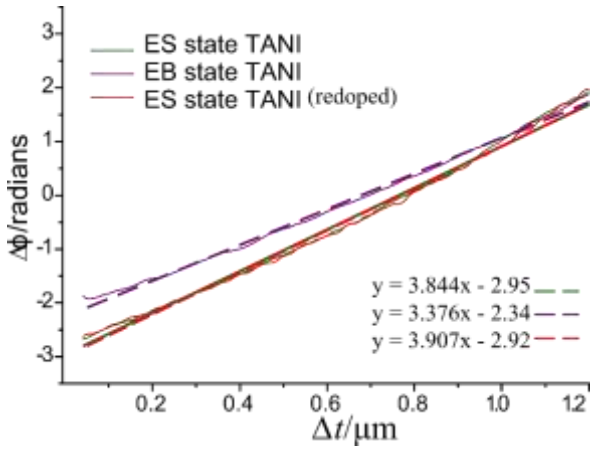

Figure S11 Figure 3d has been reproduced here with fitted slopes also presented.

Note that in contrast to the cited reference above, here the reference and signal branch use the same polarisation state in this measurement. In order to fit the gradients for the phase delay measured on the wedge-structure as a function of thickness as determined by SEM, a standard linear regression fit was made where the corresponding gradients measured are 3.844 rad/μm, 3.376 rad/μm, and 3.907 rad/μm for the doped, dedoped and redoped polymer structures,

respectively. As a measure of goodness of fit, an r^2 analysis was conducted and an r^2 value of 0.99 was found for all data sets.

S8. Simulation of the photonic band structures of the FCC woodpile structure

The photonic band structure of the woodpile structure was calculated using MIT Photonic-Bands which uses the plane-wave expansion method.[S2] The simulation were based on the dimensions of the fabricated woodpile structures: size of the unit-cell a_a = 1.800 µm, d_a = 1.273 µm, rod width w_a = 0.310 µm, rod height h_a = 0.960 µm and the overlap of the rod is 1-(a_a/4)/h_a = 53%. The rods in the woodpile structures fabricated by writing 2 lines with a 75% overlap, were replaced with single elliptical cylinders of width w_a and height h_a.

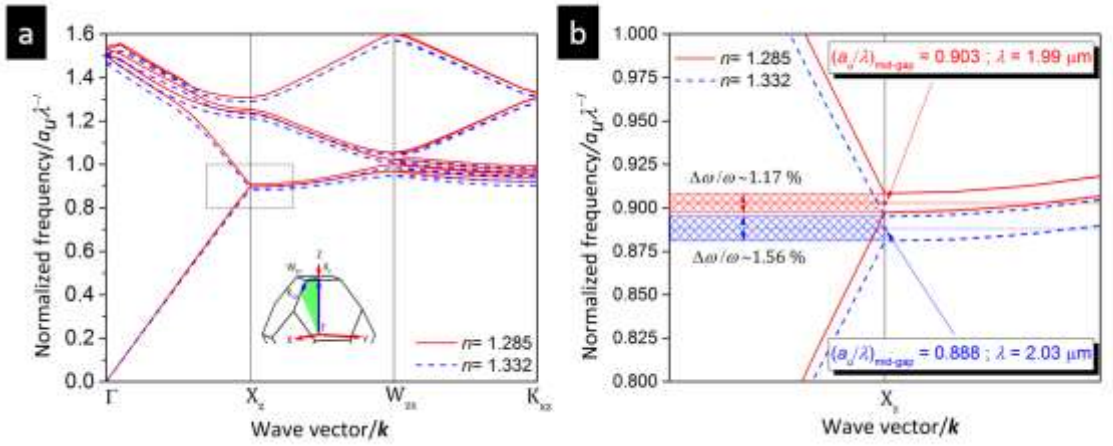

Figure S12 Photonic band diagram of the FCC woodpile photonic crystal calculated by a plane-wave method: a) band diagram from the wave vector from Γ to k_{xz} in first Brilluoin zone of the FCC reciprocal lattice and b) the enlarged band diagram around X_z wave vector, where a photonic bandgap is observed.

From the simulated photonic band diagram, a photonic bandgap is observed. The EB state woodpile structure (refractive index n_{EB} = 1.285), has a mid-bandgap at λ = 1.99 µm (the gap:midgap ratio is $(\Delta\omega/\omega)_{gap}$ = 1.17%). The ES state woodpile structure (refractive index n_{ES} = 1.332) has a mid-bandgap at λ = 2.03 µm (the gap:midgap ratio is $(\Delta\omega/\omega)_{gap}$ = 1.56%).

References

[S1] T. J. Shepherd, C. R. Brewitt-Taylor, P. Dimond, G. Fixter, A. Laight, P. Lederer, P. J. Roberts, P. R. Tapster, I. J. Youngs, *Electron. Lett.* **1998**, *34*, 787-789.

[S2] S. G. Johnson, J. D. Joannopoulos, *Opt. Express* **2001**, *8*, 173-190.